J Mater Sci (2011) 46:4397–4406
DOI 10.1007/s10853-011-5353-7

IIB 2010

# Changes in dewetting behavior of $SiO_2$ films on $TiO_2$ substrates due to film thickness and crucible choice

**Jessica L. Riesterer · C. Barry Carter**

Received: 7 June 2010 / Accepted: 31 January 2011 / Published online: 1 March 2011


**Abstract** The $TiO_2/SiO_2$ materials system has had renewed interest in recent years due to its photoelectric and photocatalytic properties, and serves as an ideal model system for liquid-phase sintering studies (LPS). In this study, glass $SiO_2$ films of three different nanoscale thicknesses were deposited onto (001) rutile $TiO_2$ substrates. The resulting dewet patterns of the glass were found to change depending on the initial film thickness when subjected to identical annealing conditions. In addition, changing the crucible type from Pt to $Al_2O_3$, caused films of the same thickness to undergo different convection mechanisms and thus developing very different surface patterns. It is proposed that Marangoni convection drove pattern formation when a Pt crucible was used, while the Rayleigh instability was responsible for dewetting when an $Al_2O_3$ crucible was used.

## Introduction

Studying dynamic behavior, such as phase separation, dissolution of phases, and convection mechanisms, can lead to the ability to tailor alloy microstructures, understand flaws in welds [1], produce improved glazes and enamels [2], and understand mass transfer in crystal growth [3], in coatings [4], and in biological applications [5, 6]. For example, convection and related instabilities have been shown to aid crack healing, pore formation, and sintering [7].

Liquid-phase sintering (LPS) depends on capillary forces in order to produce dense material at lower processing temperatures than are needed for solid-state sintering [8]. As a result, during the LPS process, glass can make up nearly 20% of the total volume of the compact [9]. Liquid at the grain boundaries allows material from one grain to dissolve and reprecipitate on the opposite grain [8, 10, 11]. However, polycrystalline specimens are complex and difficult to study. In order to isolate the wetting effects with respect to crystallography and film thickness, thin glass films are deposited onto single crystals of known orientation to provide ideal model geometries. The $SiO_2$–$TiO_2$ system, investigated here, is a model materials system for studying these effects since the materials are commonly used in industrial applications, there are few elemental components, and the phase diagram is relatively simple for a ceramic [12].

While studying these model LPS materials, interesting patterns have been found to form on surfaces and interfaces due to dewetting of the liquid phase [13]. The complex patterns are often related to the crystallography of the substrate. Understanding dewet patterns of thin films may lead to a much less expensive method of self-assembly for various applications. In addition, fewer processing steps would be needed, saving production time. Dewet patterns have been suggested for use in controlling cell growth in cancer research [14]. The behavior of self-assembled monolayers (SAMs) produced using wetting and dewetting

J. L. Riesterer · C. Barry Carter (✉)
Department of Chemical, Materials and Biomolecular Engineering, University of Connecticut, 191 Auditorium Rd. Unit 3222, Storrs, CT 06269-3222, USA
e-mail: cbcarter@engr.uconn.edu

J. L. Riesterer
e-mail: Jessica.Riesterer@inl.gov

*Present Address:*
J. L. Riesterer
Nuclear Fuels & Materials Division, Idaho National Laboratory, P.O. Box 1625, Mail Stop 6188, Idaho Falls, ID 83415-6188, USA

of polymer chains depends on the interfacial energy between the polymer and the metal or semiconductor substrate in microelectronics [15]; it is the same principles that govern dewetting in ceramics.

For this experiment, different types of dewet patterns were observed in $SiO_2$ films deposited onto rutile $TiO_2$ single-crystal substrates by changing the thickness of the initially continuous film when subjected to the same thermal treatment. By changing the crucible material used during thermal annealing, different patterns form. $TiO_2$ and $SiO_2$ together have several important applications and serve as an ideal model system for LPS studies. Multilayers of these materials serve as antireflection coatings for solar cells [16]. $TiO_2$ is a good photocatalyst [17], has high chemical stability, and is nontoxic and biocompatible [14]. $TiO_2$ has also been shown to be a promising material for water splitting and solar energy production [18]. Meanwhile, silica has good mechanical strength and high thermal stability. Additionally, the $SiO_2$–$TiO_2$ system has shown to be hydrophilic and can be useful for antifogging coatings [19].

## Background

Deposited films dewet a surface to reduce the liquid/vapor and liquid/substrate interfacial areas [20]. Liquid films need to balance three forces that are dependent on film thickness, film/substrate curvature, composition, and temperature [21]: (1) capillary forces, (2) buoyancy, and (3) hydrodynamic forces (i.e., drag) [6]. Large capillary forces can be responsible for creating holes in the film [22] and initiating dewetting. Once holes have formed in the film, exposing the substrate to the vapor, the stresses must be balanced at the solid–liquid–vapor triple point. To achieve equilibrium, the total interfacial energy must also have the smallest possible value. When the film is a liquid at high temperatures, the liquid is more reactive than the solid, and reactive wetting may alter the chemistry or surface properties of the substrate.

In 1804, Young [23] was the first to describe a dewet film or liquid on a substrate in air and recognized that a unique contact angle exists between the three phases at equilibrium. This equilibrium is related to capillary forces and hydrostatic pressure. Impurities and asperities/surface reconstruction, as described by Wulff [24] and Herring [25], on the solid surface would be able to change the behavior of the liquid due to a local change in surface tension. Likewise, Thomson [22] also discussed impurities and compositional gradients effects with respect to convection mechanisms. Young [23] also noted that a thickness limit existed. Liquid films that were thinner than a critical thickness were able to dewet, while thicker films could only completely wet the surface; i.e., films thicker than the critical value will remain as films rather than breaking apart into droplets. Capillary forces are driven by surface tension and therefore depend on the composition of the film [23]. When a critical composition exists, surface tensions and interfacial energies will adopt specific values describing an equilibrium condition [2].

For nanoscale thin films, two mechanisms may act independently or in conjunction to form complex droplet patterns. The first, being Marangoni convection, occurs when heat and mass begin to flow due to temperature and/or composition gradients. When films are heated, material can dissolve into the film from the substrate to create a composition gradient [4, 26]. Since Marangoni convection due to temperature gradients is the more commonly referenced mechanism, the description of this will be focused on here. However, composition gradients behave in a similar manner. A small temperature difference between the atmosphere (gas phase) and the substrate can prevent a liquid from wetting the surface [1]. Figure 1a illustrates Marangoni convection. In this example, the liquid at the cooler liquid–vapor interface is more viscous than at the warmer solid–liquid interface; the Marangoni force ($F_M$) drives material in the direction of the temperature gradient [1]. Equation 1 describes how $F_M$ changes for a finite particle or droplet size within the liquid film that is moving in the direction of unit vector ($n$); it is deduced by integrating over the droplet's surface forces ($S$) with respect to the film viscous stress tensor ($\tau_v$) and hydrostatic pressure ($p$). A constant temperature change, or composition change, across the liquid is assumed for Eq. 1 to remain valid.

$$F_M = \int_S n\tau_v ds - \int_S pn ds. \quad (1)$$

When films on a substrate are heated from above, the film remains in hydrostatic equilibrium. But when the temperature difference is between the cool atmosphere and the warmer substrate, the heat flow can allow Bénard cells to form in the film [27]. The cells form from the circular motion of material in the film moving from the warm substrate toward the cold surface. Bénard cells may also form from the circular motion of material trying to create a uniform density. In this way, a stable hexagonal pattern of Bénard cells forms in the surface film. The fluid moves from the solid–liquid interface through the center of the cell toward the liquid–vapor interface. Once cooled, the material flows down the edge of the cell back to the solid–liquid interface. A dimple forms in the center of the cell due to convection, in addition to surface tension [27], as shown in Fig. 1b. A perfect array of hexagonal cells will form if the system is in equilibrium, heating is uniform, and no impurities are present. When the heat flow leads to a phase transition, the instability is referred to as the Mullins–Sekerka instability [28, 29].

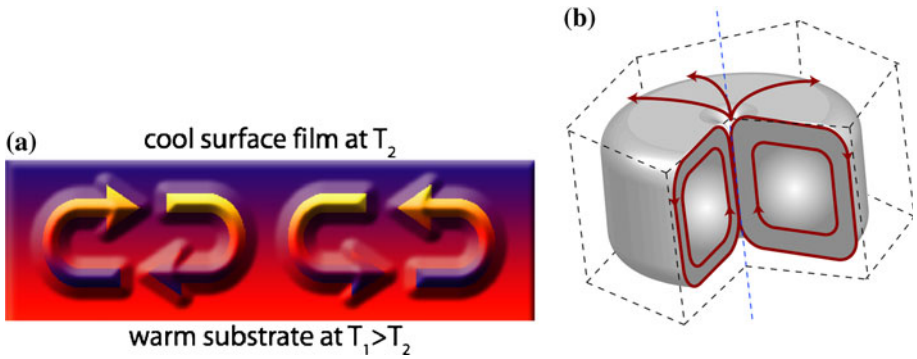


**Fig. 1** **a** Marangoni convection involves the motion of material from the bottom of the film to the top due to a temperature, composition or viscosity gradient. Marangoni forces are defined by Eq. 1. **b** Hexagonal Bénard cells form from motion of material from the center of the cell outwards. A dimple forms in the center of the cell

Factors that are seemingly independent of the glass film may cause non-equilibrium dewetting of the film. Thomson [22] realized that impurities on a substrate would alter the dewetting patterns of the liquid, while Vogel [2] proposed that the differences in density may create turbulent flow within the glass or liquid film. Vogel also proposed that the substrate could dissolve into the film to create a more dense liquid or glass. The surface energy of the film would then change, and the film would break apart into droplets.

Patterns in different materials systems have previously been observed experimentally and predicted theoretically [13, 21, 26, 28]. Pattern formation requires a seed for nucleation and a homogeneous environment [28]. The rate of growth of a pattern depends on the rate of heat transfer, or material transfer [21, 28, 30], and atmosphere [30]. Length-scales depend on both the density and surface tension of the liquid film, and dictate both droplet shape and density [21]. The presence of other nearby droplets can alter the droplet's shape [6]. When a Marangoni instability is present, temperature and compositional gradients lead to "fingers" protruding from a dewet droplet, as recently shown in metal systems by Saiz et al. [31]. Similar fingers were seen in the $SiO_2/TiO_2$ work in which the study presented here expands on; cooling rates were much slower in the previous studies, allowing more time for the complex branching and finger patterns to form [13, 21, 26]. Branching and fingers usually develop in films that exhibit secondary dewetting between the large droplets, where the droplet fingers are on the same order of magnitude as the secondary droplet height [13, 21, 26]. Since this behavior is quite complex, morphology diagrams are currently being compiled to describe transitions between complex patterns as a function of changes in variables, such as degree of undercooling and composition [28].

A second cause of nano-scale film dewetting is the Rayleigh instability, which occurs when the film or liquid is heated from below [27]. At a critical temperature, the warm material at the bottom begins to move to the top of the film and the cold material moves toward the bottom. The warm material is lighter (less dense) than the cold material, and thus sets up a density gradient, which leads to convection. Surface tension does not initially play a role in this form of convection, making it different from Marangoni convection [27]. The Rayleigh instability is more susceptible to film thickness variations, and buoyancy forces play a greater role than in Marangoni convection [4]. The Rayleigh instability will be responsible for wetting behavior at intermediate film thicknesses. For the thinnest films, van der Waals forces will control dewetting, while Bénard–Marangoni convection will control dewetting in very thick films [20].

To summarize, Rayleigh instability concerns flow internal to the film, while the Marangoni effect involves flow at the surface of the film [6]. Questions still exist as to why films/liquids initially break into droplets, hexagons, and cylinders, but substrate surface perturbations will be a contributing factor, as shown in Fig. 2. Mullins and Sekerka [29] derived expressions for capillary effects on an interface perturbation when exposed to a thermal gradient. They proposed that cell formation during solidification at a solid–liquid interface was driven by both heat and mass transport.

One possible perturbation able to induce the Rayleigh stability [32] is the degree of miscut of the substrate (the vicinal factor) [33]. If the substrate is not cut exactly parallel to a low-index plane, surface energy anisotropy may be introduced [34]. This anisotropy results in surface reconstruction upon heating, thereby altering the film's wettability. By combining the Rayleigh instability with substrate surface morphologies, dewet droplets can be tuned to produce self-assembled structures [35–38].

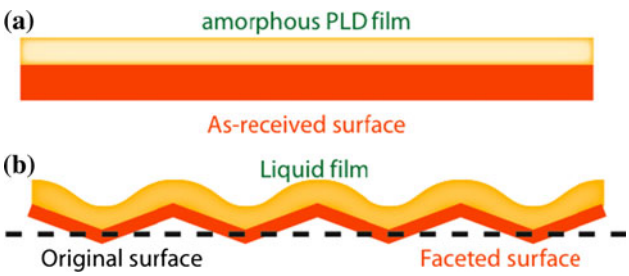


**Fig. 2** Rayleigh instability forms after **a** an initially flat, continuous film breaks apart and **b** forms droplets on top of surface features

Droplet size and surface coverage can be adjusted depending on the substrate orientation and chemical composition. Steps and hills are preferred sites for droplets, rather than terraces and valleys.

## Experimental

For this investigation of self-assembly and pattern formation during the dewetting process, $SiO_2$ glass droplets on (001) rutile-$TiO_2$ substrates were studied.

An as-received (Crystal Systems, Inc.) single-crystal (001) rutile $TiO_2$ was cut into 2 $mm^2$ pieces. Surfaces were cleaned with acetone and methanol using an ultrasonic cleaner for 10 min, respectively, prior to film deposition. Atomic force microscopy (AFM) was used to insure that as-received surfaces were highly polished and free of any notable surface features that may be a nucleation source for dewetting. Two methods were used for film deposition: pulsed-laser deposition (PLD) and plasma-enhanced chemical vapor deposition (PECVD). Films were deposited to be 50, 100, or 200 nm thick. PLD films were deposited using a KrF excimer laser operating at 248 nm wavelength, 10 Hz pulse frequency, and the chamber was under 20 mTorr of $O_2$. The substrate heater for both the PLD and PECVD was kept at 200 °C.

After film deposition, the surfaces were carefully cleaned in the same manner as mentioned above. Using a high-temperature box furnace in air atmosphere, samples were heated to 1600 °C at 20 °C/min. Samples were kept at temperature for 1 or 2 h, and removed from the furnace at temperature in order to air quench the sample and freeze the high-temperature behavior into the films. Additional films held at 1600 °C for either 1 or 2 h were allowed to cool naturally in the furnace (roughly 10 °C/min to room temperature).

Two types of crucibles were used during heat treatment. A Pt boat and lid were made by folding Pt foil. This Pt "crucible" was cleaned in phosphoric acid at 170 °C for 2 h and rinsed with distilled water before each thermal treatment. Identical heat treatments were also performed using alumina crucibles and lids. Alumina crucibles were cleaned in aqua regia (1 part hydrochloric acid: 1 part nitric acid) at room temperature until the acid stopped bubbling. The crucibles were rinsed in distilled water after acid cleaning.

AFM was used to characterize the films after deposition and after thermal treatment. Both a Park Systems XE-70 and a Digital Instruments Nanoscope III were used in contact mode with Al backside-coated Si or $Si_3N_4$ cantilevers. All cantilevers used had an approximate 10 nm radius of curvature and force constant of $\sim$0.95 N/m.

Site-specific cross-sectional samples were made using the FEI Strata Dual-beam focused ion-beam (FIB) tool operated at 30 kV. Bulk samples were coated prior to FIB milling with 50 nm of Pt to protect the surface features and reduce charging. An additional 10 nm of Pt was deposited using the electron beam in the FIB tool to prevent surface amorphization. Transmission electron microscopy (TEM) was carried out using an FEI F30 $G^2$ Ultratwin lens operated at 300 kV. High-resolution images were taken of the films to determine what occurred at the film–substrate interface. The TEM was also equipped with X-ray energy-dispersive spectroscopy (XEDS), which was used to determine the film composition; unfortunately XEDS sampled too much of the substrate to determine the quantitative film composition. Crystalline reaction layers observed in samples heated in alumina crucibles were too thin to use selected-area diffraction (SAD) to determine the crystalline phase. During TEM analysis, no features unusual to single-crystal substrates were noted in the $TiO_2$.

## Results

Different dewet patterns were observed depending on the processing conditions used and are summarized in Table 1. No difference in behavior was noted between films deposited via PECVD instead of PLD. Samples of 50-nm-thick $SiO_2$ films thermally treated in a Pt crucible resembled flowers with petals and were randomly distributed, as shown in Fig. 3. Both of the 100- and 200-nm-thick films exhibited Bénard cells with secondary droplets, with the droplets formed from the 200-nm-thick films exhibiting

**Table 1** Summary of observed dewetting dependence on initial film thickness and crucible used during thermal treatment

| Thickness (nm) | Crucible material | |
|---|---|---|
| | Pt | $Al_2O_3$ |
| 50 | Marangoni convection: square Bénard cells, minor surface sublimation pits | Sublimed film and surface |
| 100 | Marangoni convection: Bénard cells with secondary droplets [13] | Rayleigh instability: droplets residing atop facets |
| 200 | Marangoni convection: Bénard cells with extended fingers and secondary droplets [26] | Rayleigh instability: large uniform spherical droplets; incomplete dewetting |

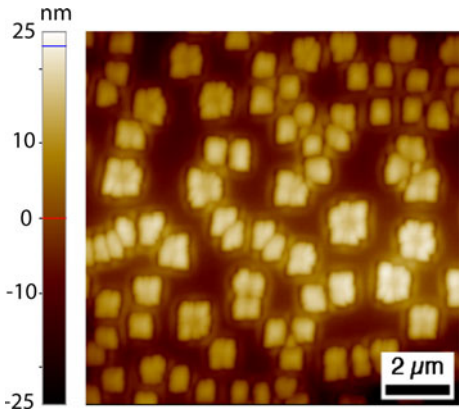


**Fig. 3** Films heated in a Pt crucible form Bénard cells of uniform size

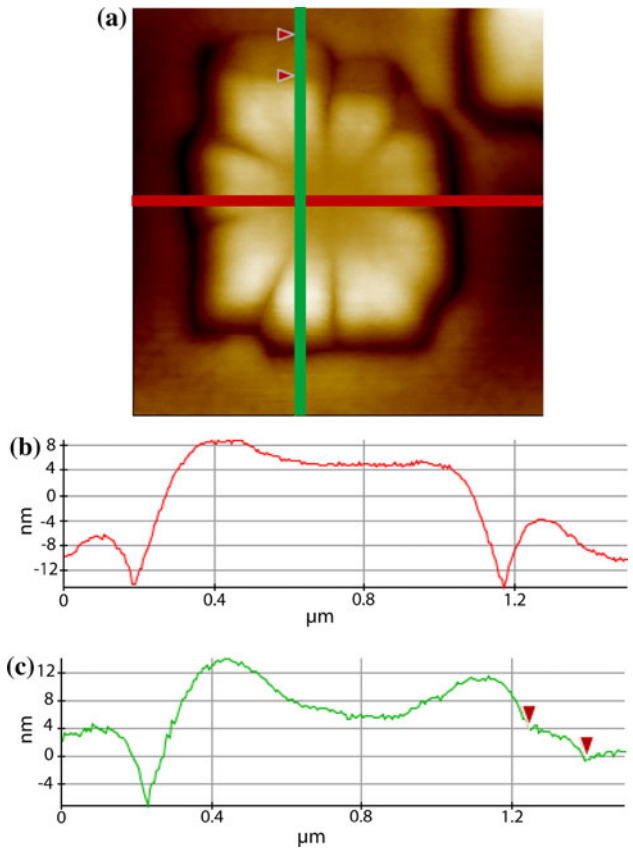


**Fig. 4** Section analyses of the Bénard cells in **a** the AFM image show a dimple present in the center and a skirt surrounds the cells. **b** Horizontal (corresponding to the *horizontal line* in **a**) and **c** vertical section analysis (corresponding to the *vertical line* in **a**)

extended fingers. Detailed results for the 100- and 200-nm-thick films heated in Pt crucibles were reported by Ravishankar and Gilliss elsewhere [13, 26, 39]. The droplets were arranged on the surface in a manner determined by the underlying crystal orientation. Section analysis of a flower-shaped droplet in Fig. 4 shows that at the center of the droplet's "petals" there is a dimple. In addition, the droplet is surrounded by a skirt or ridge of material.

When the "enhanced image" feature of the Park Systems XEI analysis software is used in Fig. 5b, small features are clearly seen to lie between the large droplets. Section analysis shows that these features are small pits in the surface. The pits were on average 3.5 nm deep, corresponding to 12 unit cells in the rutile $TiO_2$ *c*-direction [40].

The samples annealed in the $Al_2O_3$ crucibles had etched surfaces or formed droplet patterns depending on the film thickness, as shown in Fig. 6. Surface etching along crystallographic directions was observed when the initially continuous film was 50 nm thick. The dark regions in Fig. 6a are regions where etching has occurred. Surface facets have also formed. Figure 7 uses section analysis to show that facets with the classic terrace-and-ledge geometry have formed and that depressions in the surface have formed where material has been lost. Similar to the sample exposed to Pt, the surface exposed to $Al_2O_3$ had small etch pits, as seen in the inset of Fig. 7a.

When the film thickness is increased, the behavior of the samples annealed in the $Al_2O_3$ crucibles dramatically changes. When the initially continuous film was 100 nm thick and underwent the same heat treatment as the 50 nm film, the film broke up into an array of droplets and cylinders residing on top of small surface facets, as seen in Fig. 6b. The $TiO_2$ surface facets formed during the anneal. When the film thickness was increased to 200 nm, a dewetting front was observed. In Fig. 6c, the continuous film at the bottom of the image has broke apart into droplets, seen at the top of the image, with the dewetting front being in the center. A TEM cross-section was prepared from the 200-nm thickness near the front using the FIB tool. The high-resolution TEM image in Fig. 8 shows an amorphous $SiO_2$ droplet resting on top of a surface facet. A crystalline layer of $\beta$-$Al_2O_3 + TiO_2$ [12] or $\beta$-$Al_2TiO_5 + TiO_2$ [41] can be seen between the $SiO_2$ and rutile $TiO_2$. EDS was used to determine the qualitative composition of the layers.

## Discussion

### Dependence on crucible material

Instead of a regular pattern of droplets, the films heated in the Pt crucible broke apart into random flower-shaped patterns; such patterns are typically observed in polymeric films and organic solutions [1, 15, 21, 42, 43]. However, the droplets in Fig. 3 did exhibit a texture related to the (001) rutile $TiO_2$ surface below. The surface tension is

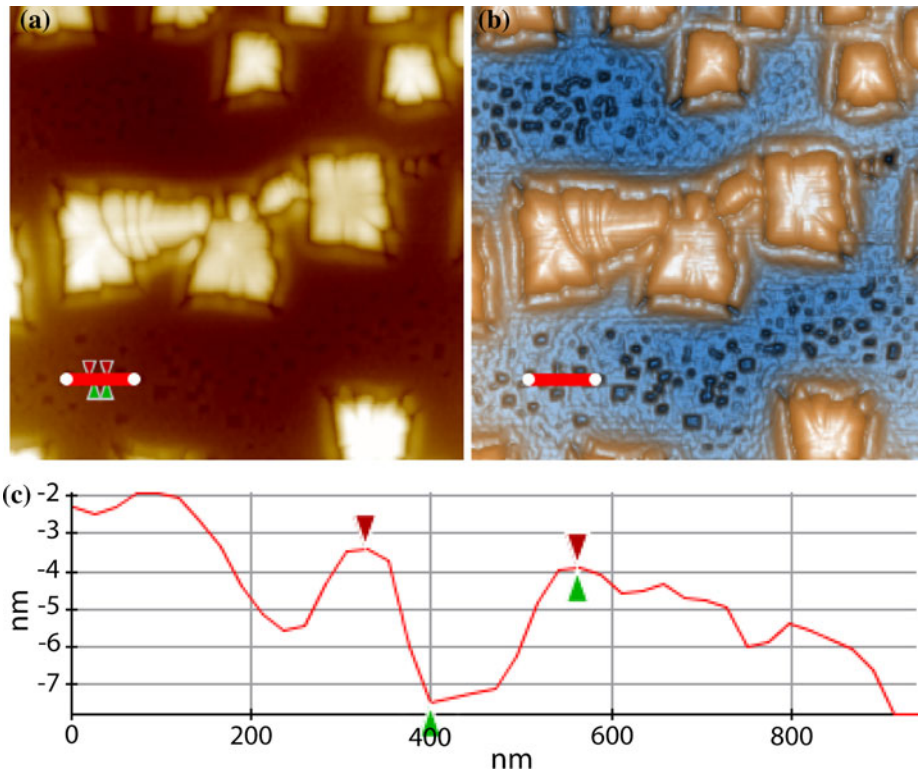


**Fig. 5** Surface pits in samples annealed in a Pt crucible are easily seen in **b** an enhanced color AFM height image (similar to a plotted topographic map) and **c** section analysis, while not as clearly shown in **a** the traditional AFM image

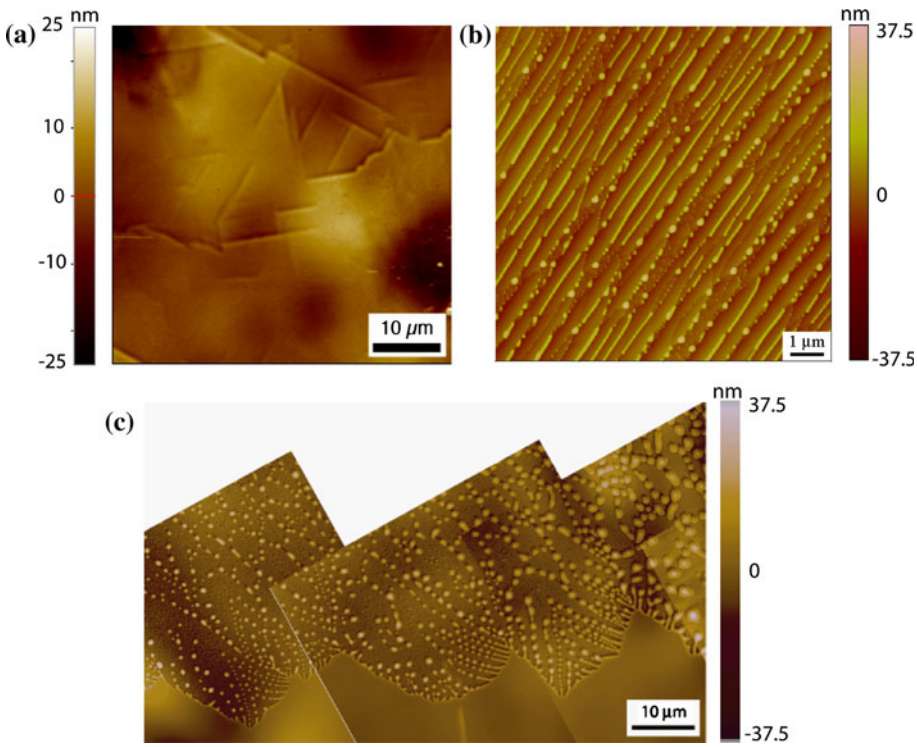


**Fig. 6** Films annealed in an $Al_2O_3$ crucible for 1 h at 1600 °C; **a** 50 nm thick, **b** 100 nm thick, and **c** 200 nm thick $SiO_2$ on (001) rutile $TiO_2$ (note the different magnifications)

lower in low-index directions, and this influences the shape of the droplets.

The droplet shown at higher magnification in Fig. 4 is a clear example of Marangoni convection. Comparing Figs. 1b and 4a, the droplets have formed square Bénard cells by dissolving the rutile substrate into the $SiO_2$ film at temperature. The change in density and composition forms a gradient, which drives convection while the sample is at temperature. Upon cooling, the glass becomes supersaturated and the $TiO_2$ must precipitate out of solution, forming

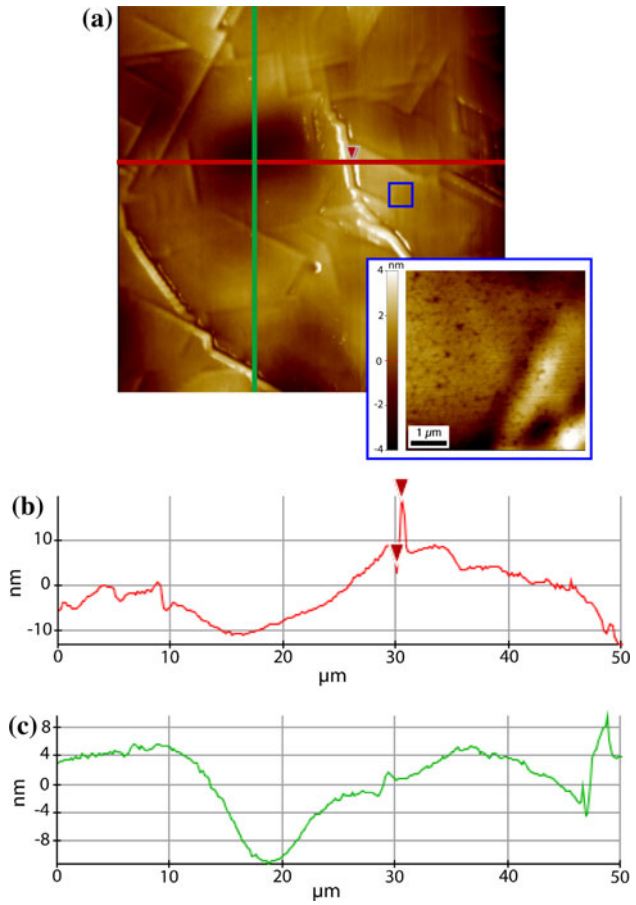


**Fig. 7** Section analysis of 50 nm thick film heated in an $Al_2O_3$ crucible shows surface facets and large depressions on the surface in the **a** AFM image. *Inset* in **a** shows small surface pits covering the surface. **b** Horizontal section analysis (corresponding to the *horizontal line* in **a**); **c** vertical section analysis (corresponding to the *vertical line* in **a**)

the epitactic humps at the interface [26]. (The process is actually liquid-phase epitactic growth/crystallization [44] of rutile.) While composition homogenization will occur while at the anneal temperature, the liquid becomes super-saturated on cooling. The excess $TiO_2$ must come out of solution during cooling, and this is what sets up the composition gradients and dewetting. Therefore, homogenization during annealing does not effect the dewetting. Ravishankar [13] and Gilliss [26] proved this by changing the cooling rate for the same materials system and observing differing dewet patterns. The density of $SiO_2$ changes with the addition of $TiO_2$ according to $r_{TiO_2} = 3.7611 - 0.00028T$ °C for the temperature range of 1600 to 1925 °C [45]. It is thus the $TiO_2$ coming out of solution that forms the skirt seen in the section analyses of the droplet in Fig. 4b and c. FIB sections have shown that $TiO_2$ humps and skirts have formed near the edge of droplets [13], supporting Vogel's theory [2] and this work.

Contact angles in sessile drop experiments have been shown to depend on the size of the droplet due to gravity and surface energy [46]. In this case, surface energy would be the influencing factor since gravity is negligible in thin films. Since all of the formed droplets result in having the same length scale in this study, droplet size must be an important factor in overall pattern formation. More regular hexagonal patterns in the same materials system has been previously observed in thicker films [13]. It is proposed here that with a thinner glass film, any substrate space charge will have a greater effect in pattern formation than when the film is thick. Space charge can be a very influential factor at small length-scales and, therefore, may help to dictate which type of droplet pattern forms on the substrate surface.

Using an $Al_2O_3$ crucible rather than Pt for the exact same heat treatment on a film of the same thickness gives a dramatically different result. Droplets of $SiO_2$ could not be found on the surface after thermal treatment for samples that originally included 50-nm-thick continuous films. Rather, the surface has large facets that are not in a regular array, as usually expected for surface reconstruction [47]. Figure 7 shows the cross-section of a representative area;

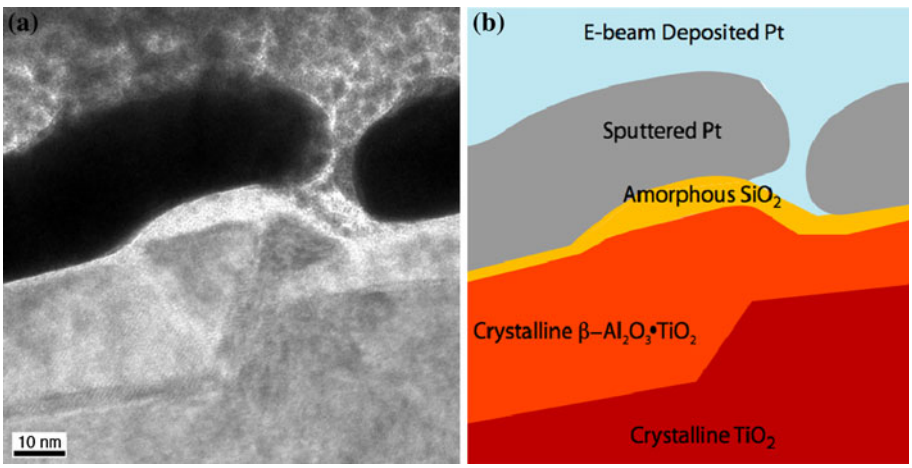


**Fig. 8** **a** HRTEM and **b** schematic of a FIB cross-section showing the reaction layer of $Al_2O_3$ contaminates determined via EDS

along with the facets, depressions have formed. Sublimation of $Al_2O_3$ during processing of ceramic materials has been long known [48, 49]; the surface of the $Al_2O_3$ crucible sublimes on heating and introduces impurities into the liquid film. Altering of the surface tension of the upper layer of a glass film due to changes in atmosphere, the oxygen partial-pressure in particular, have been reported [2]. In this case, the thin as-deposited $SiO_2$ film may have completely sublimed and/or a continuous reaction product film formed between $TiO_2$, $SiO_2$, and $Al_2O_3$. The combination of atmosphere, impurities, and sublimation of the film and the surface would furthermore change the surface reconstruction behavior of the rutile substrate. In addition, reactive wetting of Al on $TiO_2$ has been previously reported; the effect of the reaction is to cause the wetting angle to change depending on (i) Al, Ti, and O concentrations in the liquid and (ii) the oxygen partial pressure of the furnace atmosphere [50].

The observations in the inset of Fig. 7a confirm this hypothesis. The small dark features are etch pits in the surface. The facets in Fig. 7 are irregular due to surface energy considerations [47]. Small etch pits were also observed in the films heated in a Pt crucible, but to a much lesser extent, as seen in Fig. 5. While no $Al_2O_3$ was intentionally placed near the samples during heat treatment, the furnace insulation may have contributed enough impurities to allow sublimation of the surface. More work is needed to fully understand the effect of $Al_2O_3$ on the $TiO_2$ surface.

## Dependence on film thickness

When the thickness of the film increases, the film remains, but is markedly different from when a Pt crucible is used: small additions of impurities to a glass film can significantly alter the surface tension of the film [2].

In films that were initially 100 nm thick, as shown in Fig. 6b, the Rayleigh instability caused the film to break apart. Upon heating, the underlying substrate began to reconstruct. When the surface facets change the local thickness of the now liquid film, the film breaks apart into cylinders and, later, droplets of the same diameter. The cylinders and droplets of glass reside on the tops of the facets. While observed for metal [35, 37] and polymeric glass [43] films on reconstructed ceramic substrates, these patterns have not been previously observed for glass on a ceramic substrate.

When the film was initially 200 nm thick, dewetting occurred more slowly than in the films that were initially 100 nm thick. The continuous film at the bottom of the montage of AFM images in Fig. 6c breaks apart into cylinders and trails of droplets seen at the top of the image. These droplets form a regular array of droplets, and mimic behavior seen in polystyrene films on Si wafers [43]. The "front" formed as a thin liquid film dewets a surface may be thought of as being the interface between a two-phase region (solid and liquid) growing into a single-phase (liquid only) region on an initially smooth interface; i.e., the surface prior to surface reconstruction nucleation, as described by the Mullins–Sekerka instability [28, 29]. Dewetting starts as the nucleation and growth of a "dry" area with a receding liquid front that eventually breaks into fingers which then break into smaller droplets due to Rayleigh instabilities. Marangoni forces still affect such solidification fronts by causing the droplets to repel each other [6], but other factors, such as surface faceting, may be contributing to the pattern formation. Dewetting area versus time is not needed here. Since the entire surface of the 100 nm films were completely dewet, while the 200-nm thick film surface was only partially dewet and still had patches of continuous film, and both were annealed and cooled for exactly the same time, the conclusion is that the thicker film takes longer to dewet. In other words, more volume of material will take longer to break apart. In addition, the number of impurities per unit volume will be lower for thicker films than thinner films due to diffusion/absorption of the impurities when held at temperature for the same length of time. Therefore, the initial film thickness is an important factor in determining the dewetting behavior and resulting droplet patterns of glass films and a critical film thickness is implied.

As mentioned previously, $Al_2O_3$ was confirmed to be present in the samples heat-treated in an $Al_2O_3$ crucible. Figure 8 illustrates the composition determined using EDS during high-resolution TEM in scanning transmission (STEM) mode. Initially, the deposition method, PECVD versus PLD, was thought to introduce the impurities. However, impurities were actually introduced from the sublimation of material forming the crucibles; this interpretation was confirmed when films deposited via each technique were annealed separately in the other type of crucible; the dewetting behavior was exactly the same when the same crucible type was used.

The $Al_2O_3$ found between the $SiO_2$ and $TiO_2$ layers is introduced by sublimation of the high-purity crucible during heat treatment followed by diffusion through the $SiO_2$ liquid. Numerous authors (e.g., Sata and Sasamoto [51]) have found that $Al_2O_3$ will vaporize when heated to high temperatures ($\geq$1800 °C) and/or under vacuum ($10^{-2}$ to $10^{-3}$ Pa). The presence of other phases or impurities is thought to decrease the temperature and vapor pressure needed for $Al_2O_3$ to sublime. An Al–Ti–O reaction product has been previously observed during sessile drop wetting experiments [50]. Upon cooling, the reaction product will come out of solution in crystalline form in a manner similar to 200 nm thick $SiO_2$ films on $TiO_2$ heated in Pt crucibles

undergoing Marangoni convection [39]. The structure of the reaction layer shown in Fig. 8 was ambiguous, being either $\beta$-$Al_2O_3$ + $TiO_2$ [12] or $\beta$-$Al_2TiO_5$ + $TiO_2$ [41]. The ternary phase diagram was not helpful here, since the amount of Al in the reaction layer could not be measured and only diagrams for temperatures higher than the anneal temperature could be found. Bench et al. [52] grew $TiO_2$ on $Al_2O_3$ using PLD. The epitactic film gave diffraction patterns that were not identifiable due to being to thin for SAD analysis and too much of the substrate being sampled during XEDS, as is the case here. Phases were thought to be nonstoichiometric $TiO_{2-x}$ or a reaction layer between $TiO_2$ and $Al_2O_3$.

## Conclusions

In this work, dewet patterns of $SiO_2$ glass on rutile $TiO_2$ substrates were found to depend on the type of crucible used during heat treatment and the thickness of the initial continuous film. The mechanisms responsible for the patterns are Marangoni and Rayleigh convection; these processes are quite well known in polymeric films and organic solutions, but not as common in traditional materials science. Both types of convection are driven by gradients in composition and viscosity. Films brought to temperature in Pt crucibles showed Marangoni convection and the formation of Bénard cells dependent on the substrate surface tension. Rayleigh convection was observed when films were heated in the presence of $Al_2O_3$. The surface in both cases was observed to sublime when the glass film was very thin, but to a lesser extent in films heated in Pt crucibles. The thickness of the film determined whether the film would sublime to leave irregular surface facets, form a uniform array of droplets, or be caught in the initial dewetting of the continuous film. Therefore, by simply changing crucible type and/or film thickness, surface patterns of dewet glass films may potentially be tuned for desired properties.

More importantly, these experiments have shown that by changing seemingly minor processing conditions, the resulting patterns can be dramatically different. An enormous range of experiments have yet to performed to further elucidate this behavior; however, this study emphasizes that chosen processing conditions, such as crucible choice, are often not chosen carefully enough, and acts as a word of caution to all researchers.

**Acknowledgements** The authors would like to thank the University of Connecticut and the 3M Harry Heltzer Endowed Multidisciplinary Chair at the University of Minnesota for funding part of this work. Thanks are due to Dr. Christopher R. Perrey for his help with TEM and EDS and to Dr. Shelley R. Gilliss, Prof. N. (Ravi) Ravishankar, and Dr. William M. Mook for many thought-provoking discussions.

## References

1. Monti R, Savino R, Alterio G (2002) Acta Astronaut 51:789
2. Vogel W (1971) Structure and crystallization of glasses. Pergamon Press, Leipzig, pp 134
3. Nakanisi H, Watanabe M, Terashima K (2002) J Cryst Growth 236:523
4. Kumar S, Roy S (2006) Numer Heat Transf A 50:689
5. Böcking D, Fiedler J, Brenner RE, Hüsing (2009) J Mater Sci 44:6786. doi:10.1007/s10853-009-3565-x
6. Velarde MG (1998) In: Hondros ED, McLean M, Mills KC (eds) Marangoni and interfacial phenomena in materials processing. IOM Communications, London, p 15
7. Santala MK, Glaesar AM (2006) Surf Sci 600:782
8. German RM, Suri P, Park SJ (2009) J Mater Sci 44:1. doi:10.1007/s10853-008-3008-0
9. Susnitzky DW, Kouh Simpson Y, DeCooman BC, Carter CB (1986) Mat Res Soc Symp Proc 60:219
10. Burke JE (1957) J Am Ceram Soc 40:80
11. Rossi G, Burke JE (1973) J Am Ceram Soc 56:654
12. DeVries RC, Roy R, Osborn EF (1954) Trans J Br Ceram Soc 53:525
13. Ravishankar N, Gilliss SR, Carter CB (2003) J Eur Ceram Soc 23:2777
14. Kang BS, Ren F, Jeong BS, Kwon YW, Baik KH, Norton DP, Pearton SJ (2005) J Vac Sci Technol B 23:57
15. Ferguson GS, Whitesides GM (1991) In: Schrader ME, Loeb G (eds) Modern approach to wettability: theory and applications. Plenum Press, New York, p 143
16. Lien S-Y, Wuu D-S, Yeh W-C, Liu J-C (2006) Sol Energy Mater Sol C 90:2710
17. Mei F, Liu C, Zhang L, Ren F, Zhou L, Zhao WK, Fang YL (2006) J Cryst Growth 292:87
18. Noguera C (1996) Physics and chemistry at oxide surfaces. Cambridge University Press, Cambridge
19. Fujimoto M, Ohno T, Suzuki H, Koyama H, Tanaka J (2005) J Am Ceram Soc 88:3264
20. Callegari G, Calvo A, Hulin J-P, Brochard-Wyart F (2002) Langmuir 18:4795
21. Besancon BM, Green PF (2004) Phys Rev E 70:224903
22. Thomson J (1855) Philos Mag 10:330
23. Young T (1805) Philos Trans R Soc Lond 95:65
24. Wulff G (1901) Z Kristallogr 34:449
25. Herring C (1951) Phys Rev 82:87
26. Gilliss SR (2004) Ceramic oxides: surfaces and amorphous/crystalline interfaces. Ph.D., University of Minnesota
27. Koschmieder EL (1993) Bénard cells and Taylor vortices. University of Cambridge, Cambridge
28. Brener E, Mÿller-Krumbhaar H, Temkin D, Abel T (2000) Solid State Ionics 131:23
29. Mullins WW, Sekerka RF (1963) J Appl Phys 34:323
30. Bechelany M, Maeder X, Riesterer JL, Hankache J, Lerose D, Christiansen S, Michler J, Philippe L (2010) Cryst Growth Des 10:587
31. Saiz E, Benhassine M, De Coninck J, Tomsia AP (2010) Scripta Mater 62:934
32. Rayleigh JWS (1878) Proc Lond Math Soc 10:4
33. de Gennes PG (1985) Rev Mod Phys 57:827
34. Riesterer JL (2009) Reconstructing oxide surfaces. Ph.D., University of Minnesota
35. Basu J, Carter CB, Divakar R, Mukherjee B, Ravishankar N (2009) Appl Phys Lett 94:171114
36. Gai Z, Howe JY, Blom DA, Plummer EW, Shen J (2005) Appl Phys Lett 86:1
37. Lødziana Z, Norskov JK (2002) Surf Sci Lett 518:L577

38. Ravishankar N, Shenoy VB, Carter CB (2004) Adv Mater 16:76
39. Gilliss SR, Ravishankar N, Kotula PG, Michael JR, Carter CB (2002) Microsc Microanal 8:562
40. Carter CB, Norton MG (2007) Ceramic materials: science and engineering. Springer, New York
41. Musil J, Šatava V, Čerstvý ZemanP, Tölg T (2008) Surf Coat Technol 202:6064
42. Heine DR, Grest GS, Webb EB III (2005) Langmuir 21:7959
43. Reiter G (1993) Langmuir 9:1344
44. Lorenz MR (1963) J Appl Phys 36:2908
45. Dingwell DB (1991) J Am Ceram Soc 74:2718
46. Spelt JK, Li D, Neumann AW (1991) In: Schrader ME, Loeb G (eds) Modern approach to wettability: theory and applications. Plenum Press, New York, p 101
47. Mullins WW (1961) Philos Mag 6:1313
48. Brewer L, Searcy AW (1951) J Am Chem Soc 73:5308
49. Wang ZL, Bentley J (1993) Ultramicroscopy 51:64
50. Avraham S, Kaplan WD (2005) J Mater Sci 40:1093. doi: 10.1007/s10853-005-6922-4
51. Sata T, Sasamoto T (1984) In: Kingery WD (ed) Structure and properties of MgO and $Al_2O_3$ ceramics. The American Ceramic Society, Columbus, OH, p 541
52. Bench MW, Kotula PG, Carter CB (1997) Surf Sci 391:183